PHYSICAL REVIEW B **84**, 054408 (2011)

High-field magnetic phase transitions and spin excitations in magnetoelectric $LiNiPO_4$

Rasmus Toft-Petersen,[1] Jens Jensen,[2] Thomas Bagger Stibius Jensen,[1] Niels Hessel Andersen,[1] Niels Bech Christensen,[1,3]
Christof Niedermayer,[3] Michel Kenzelmann,[4] Markos Skoulatos,[5] Manh Duc Le,[5] Kim Lefmann,[2,6] Sonja Rosenlund Hansen,[2]
Jiying Li,[7] Jerel L. Zarestky,[7] and David Vaknin[7]
[1]*Materials Research Division, Risø DTU, Technical University of Denmark, DK-4000 Roskilde, Denmark*
[2]*Niels Bohr Institute, Universitetsparken 5, DK-2100 Copenhagen, Denmark*
[3]*Laboratory for Neutron Scattering, Paul Scherrer Institute, CH-5232 Villigen, Switzerland*
[4]*Laboratory for Developments and Methods, Paul Scherrer Institute, CH-5232 Villigen, Switzerland*
[5]*Helmholtz Zentrum Berlin for Materials and Energy, Hahn-Meitner-Platz 1, D-14109 Berlin, Germany*
[6]*Nano-Science Center, Niels Bohr Institute, Universitetsparken 5, DK-2100 Copenhagen, Denmark*
[7]*Ames Laboratory and Department of Physics and Astronomy, Iowa State University, Ames, Iowa 50011, USA*

(Received 20 January 2011; published 2 August 2011)

The magnetically ordered phases and spin dynamics of magnetoelectric $LiNiPO_4$ have been studied in fields up to 17.3 T along the c axis. Using neutron diffraction, we show that a previously proposed linearly polarized incommensurate (IC) structure exists only for temperatures just below the Néel temperature T_N. The ordered IC structure at the lowest temperatures is shown instead to be an elliptically polarized canted spiral for fields larger than 12 T. The transition between the two IC phases is of second order and takes place about 2 K below T_N. For $\mu_0 H > 16$ T and temperatures below 10 K, the spiral structure is found to lock in to a period of five crystallographic unit cells along the b axis. Based on the neutron-diffraction data, combined with detailed magnetization measurements along all three crystallographic axes, we establish the magnetic phase diagrams for fields up to 17.3 T along c and for fields up to 16 T along a and b. The spin excitations in the high-field IC spiral phase have been studied in detail by inelastic neutron scattering. A mean-field analysis shows that the spin Hamiltonian derived previously from the low-temperature spin waves at zero field predicts the transition between the linear and elliptical polarization of the IC structure, and that a generalization of the spin-wave theory, assuming the random-phase approximation, accounts for the inelastic scattering data obtained in the commensurable uniform phase at fields below 12 T as well as those obtained in the high-field IC spiral phase.

DOI: 10.1103/PhysRevB.84.054408 PACS number(s): 75.25.−j, 75.10.Dg

I. INTRODUCTION

Materials with coexisting ferroic order parameters—the so-called multiferroics—have received much attention in recent years.[1,2] Some of these multiferroics exhibit a magnetoelectric (ME) coupling, where an applied magnetic field induces an electric polarization and vice versa.[3] In some of these cases the magnetic ordering temperature and the onset temperature of the ME effect are identical and ferroelectricity is generated by the long-range magnetic order being perturbed by the magnetic field.[4–7] The *lithium-ortho-phosphates* $LiMPO_4$ (M = Mn, Co, Fe, or Ni) are isostructural compounds that all exhibit a strong ME effect in their low-temperature commensurate (C) antiferromagnetic (AFM) phases.[8–10] $LiNiPO_4$ stands out among the lithium-ortho-phosphates by exhibiting incommensurate (IC) magnetism, suggesting the presence of competing magnetic interactions. This expectation was confirmed directly by inelastic neutron scattering in Ref. 11.

The $LiNiPO_4$ compound has orthorhombic symmetry with space group $Pnma$ (No. 62) and lattice parameters $a = 10.02$ Å, $b = 5.83$ Å, and $c = 4.66$ Å.[12] There are four magnetic Ni^{2+} ions in each unit cell with spin $S = 1$. At zero magnetic field the system displays long-range AFM order at temperatures below $T_N = 21.7$ K,[13] while short-range IC magnetic order exists in the temperature range $T_N < T < 40$ K.[14] Between T_N and $T_{NC} = 20.8$ K, $LiNiPO_4$ exhibits spontaneous IC magnetic order with ordering wave vector $\mathbf{k}_{ic} = (0,k_{ic},0)$.[7,14–16] Below T_{NC}, the AFM structure is commensurate with the lattice in the sense that the magnetic and crystallographic unit cells are identical. In this phase, the ordered moments are almost parallel to the crystallographic c axis with a slight canting along the a axis,[7,13] as shown schematically in Fig. 1. The small canting is responsible for the ME effect observed in the commensurate phase when a field is applied along the a or c axes,[8,9,14] according to the model developed in Ref. 7. A magnetic field applied along the c axis induces a first-order C to IC phase transition at a field strength $\mu_0 H$ varying between 12 and 13.5 T depending on temperature.[7] In Ref. 7, the high-field IC structure at low temperatures, like the zero-field IC structure observed between T_N and T_{NC}, was suggested to be linearly polarized, but it was also pointed out that the data did not exclude an elliptical polarization. The matter was left unresolved, since no direct evidence for a spiral structure was observed.

The low-temperature C–IC phase transition is the first out of the five magnetic-field induced transitions observed by Khrustalyov *et al.*[17] as peaks in the differential magnetic susceptibility dM/dH derived from magnetization measurements in pulsed magnetic fields extending up to 27 T along the c axis. A second transition at $\mu_0 H \approx 16$ T gives rise to a much smaller peak in dM/dH than the C–IC transition.

In this paper, we present neutron-diffraction studies as a function of temperature and magnetic fields up to 17.3 T clarifying the structures of the IC magnetic phases of $LiNiPO_4$. The high-field, low-temperature IC magnetic structure is shown to be a canted, elliptical spiral with the spin components rotating in the crystallographic ac plane. This structure undergoes a temperature-driven transition to a canted,

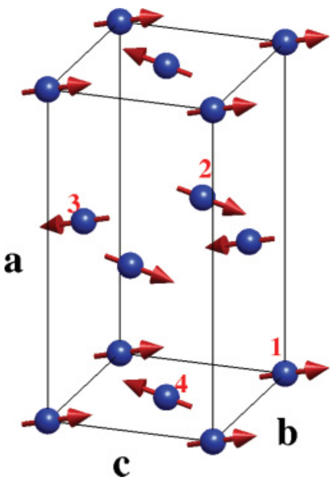

FIG. 1. (Color online) The zero-field commensurate magnetic structure of $\mathrm{LiNiPO_4}$ observed below T_{NC}. The magnetic unit cell is shifted (−0.25,−0.25,0) with respect to the structural unit cell. The magnetic ion positions are numbered 1–4 (after Ref. 7).

linearly polarized structure, where all moments are nearly parallel or antiparallel to the c axis. At fields larger than 16 T and temperatures below 10 K, the low-temperature IC spiral conforms to a commensurate quintupling of the crystallographic unit cell along the b axis corresponding to an ordering wave vector $(0,\frac{1}{5},0)$. To assist the neutron-diffraction determination of the phase boundaries for fields along c, we have performed detailed magnetization measurements up to 16 T. The combined data are used to present the full $(\mu_0 H,T)$-phase diagram for fields up to 17.3 T. Magnetization measurements for fields up to 16 T along the a and b axes have been used to establish the corresponding $(\mu_0 H,T)$-phase diagrams.

Furthermore, we have studied the low-temperature spin excitation spectrum in the spiral IC phase as well as field and temperature dependent properties of the spin excitations in the commensurate low-temperature phase by inelastic neutron scattering. The data are analyzed within the random-phase approximation (RPA) in terms of the spin Hamiltonian established in Ref. 11. The mean-field (MF) predictions derived from the same spin Hamiltonian are compared with the experimental results for the zero-field susceptibilities, the phase diagram, and the magnetic structures.

The paper is organized as follows: In the next section, an account of the irreducible representations of the magnetic structures in $\mathrm{LiNiPO_4}$ is given. This is succeeded by a description of the experimental determination of the magnetic phases in Sec. III, where complete $(\mu_0 H,T)$ phase diagrams for fields along all three crystallographic directions will be presented. The neutron diffraction data from experiments at RITA-II (III B) and FLEX/V2 (III C) spectrometers are presented along with the bulk magnetization data in Sec. III D. The structural part of the paper is followed by a description of the MF model and the RPA in Sec. IV A. In Sec. IV B, we present experimental results for the spin-wave excitations in the high-field IC spiral phase obtained at RITA-II. These results are compared with the predictions of the RPA model. Concluding remarks are given in Sec. V.

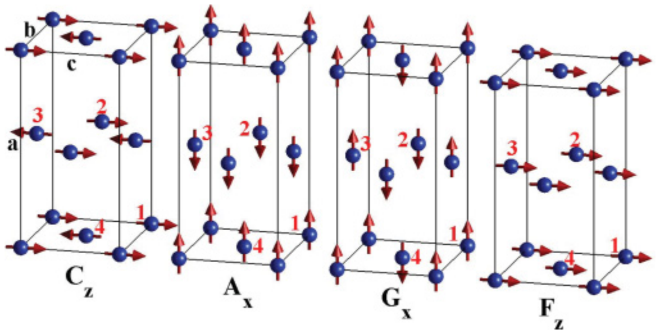

FIG. 2. (Color online) Four of the twelve commensurate irreducible basis structures related to the three AFM symmetry classes (A, G, and C) and the ferromagnetic class (F). Only one of the three possible polarizations (x,y,z) is shown for each one of the four different classes.

II. MAGNETIC STRUCTURES IN $\mathrm{LiNiPO_4}$

The four magnetic ions in $\mathrm{LiNiPO_4}$ are situated at $\mathbf{r}_1 = (0.275,0.25,0.98)$, $\mathbf{r}_2 = (0.775,0.25,0.52)$, $\mathbf{r}_3 = (0.725,0.75,0.02)$, and $\mathbf{r}_4 = (0.225,0.75,0.48)$ in the orthorhombic unit cell (see Fig. 1). A thorough analysis of the irreducible representations[18] of the magnetic structures in $\mathrm{LiNiPO_4}$ has been performed in Ref. 15. In the uniform case, i.e., when the magnetic and the crystallographic unit cells are identical, any magnetic structure is described by a linear combination of the twelve basis structures presented in Fig. 2. This basis is divided into four symmetry classes (A, C, G, and F) for each Cartesian component of the moments. In the IC phases, where the ordering wave vector is $\mathbf{k}_{\mathrm{ic}} = (0,k_{\mathrm{ic}},0)$, the same basis applies except that it includes a phase factor $\beta = e^{i\pi k_{\mathrm{ic}}}$ due to the modulation of the moments. The Fourier transforms of the spin components may be divided into the four symmetry classes $A_\alpha = (+,-,-\beta,+\beta)$, $G_\alpha = (+,-,+\beta,-\beta)$, $C_\alpha = (+,+,-\beta,-\beta)$, and $F_\alpha = (+,+,+\beta,+\beta)$, where the brackets show the relative phase factors of the α component of the spins on the sites $(\mathbf{r}_1,\mathbf{r}_2,\mathbf{r}_3,\mathbf{r}_4)$ in one unit cell. α is equal to x,y, or z, where these axes are along, respectively, the a, b, and c axes of the lattice.

These basis structures span the space of possible IC magnetic structures in $\mathrm{LiNiPO_4}$, when the ordering wave vector $\mathbf{k}_{\mathrm{ic}}$ is along the b axis. The symmetry operations of the space group $Pnma$ that leave $\mathbf{k}_{\mathrm{ic}}$ invariant (excluding lattice translations) constitute the little group $G_{\mathbf{k}_{\mathrm{ic}}} = \{1,2'_y,m'_{xy},m'_{yz}\}$. There are four one-dimensional irreducible representations, Γ_1–Γ_4, of this little group. The twelve IC basis structures are divided into corresponding subsets according to how they transform under the symmetries of $G_{\mathbf{k}_{\mathrm{ic}}}$. These subsets are

$$\begin{aligned} &\Gamma_1\colon\{A_x,G_y,C_z\} \quad \Gamma_2\colon\{G_x,A_y,F_z\} \\ &\Gamma_3\colon\{C_x,F_y,A_z\} \quad \Gamma_4\colon\{F_x,C_y,G_z\}. \end{aligned} \tag{1}$$

If a magnetic IC structure is found to involve a component from one of the irreducible representations (for instance C_z), it is more or less inevitable that it also involves the two other components (A_x and G_y).

III. MAGNETIC PHASES OF LiNiPO$_4$ AT HIGH MAGNETIC FIELDS

A. Experimental details

Two high-quality single crystals measuring $5 \times 5 \times 9$ mm^3 (0.4 g) and $2 \times 2 \times 3$ mm^3 (0.02 g), respectively, were used in the experiments. Both elastic and inelastic neutron scattering experiments were performed on the RITA-II triple-axis spectrometer at the Paul Scherrer Institute (SINQ, PSI) using the larger crystal oriented on an aluminum sample holder with the c axis vertical in a 14.9 T Oxford cryomagnet. No collimation was used. For inelastic scattering, varying incoming neutron energy was used with fixed neutron momentum transfer $\mathbf{Q}$ and fixed final neutron energy of 5 meV. A Be filter was placed before the analyzer to remove higher order neutrons. RITA-II has a seven-blade pyrolytic graphite (PG) analyzer providing high q-resolution, when measuring the dispersion along $(0,q,0)$. When measuring the dispersions along $(q,1,0)$ and $(q,1+k_{\mathrm{ic}},0)$, the intensity from only the three central blades was collected. The diffraction studies were performed with 4.04 Å (5 meV) neutrons using only the central blade. On the V2/FLEX triple-axis spectrometer at Helmholtz Zentrum Berlin neutron diffraction was performed for magnetic fields up to $\mu_0 H = 17.3$ T. The smaller crystal was placed with the c axis vertical in an aluminum sample holder clamping it between two Dysprosium booster pieces, which add 2.5 T to the field provided by a 14.8 T Oxford cryomagnet. We used 4.04 Å neutrons, a flat PG analyzer, and 60′ collimation between monochromator and sample, sample and analyzer, as well as between the analyzer and the detector. A CRYOGENIC cryogen free measurement system (CFMS) at Risø DTU was used to perform vibrating sample magnetization (VSM) measurements. Magnetic fields $0 \leqslant \mu_0 H \leqslant 16$ T were applied along all three principal axes for temperatures $2 < T < 300$ K. Susceptibilities are measured at $\mu_0 H = 1$ T, which lies within the linear regime of magnetization vs field.

B. The transition between IC structures with different polarizations

The previously determined high-field IC structure with ordering wave vector $(0,k_{\mathrm{ic}},0)$ had basically C_z symmetry with a small A_x canting plus small uniform F_z and G_x components induced by the field.[7,15] It was argued that the IC structure was this canted structure with the moments polarized linearly nearly along z, but that it could also be a spiral with spins rotating in the ac plane. To examine whether this is the case, we have used the RITA-II spectrometer to measure the temperature dependence of three magnetic IC peaks $(0,1+k_{\mathrm{ic}},0)$, $(1,k_{\mathrm{ic}},0)$, and $(1,2+k_{\mathrm{ic}},0)$ at 14.7 T.

The sensitivity of neutron scattering to magnetic structures is a consequence of a scattering cross section which, for a collinear structural component, is proportional to $|F_R(\mathbf{Q})|^2 |P(\mathbf{Q})|^2$, where the structure (F) and polarization (P) factors are given by

$$F_R(\mathbf{Q}) = \sum_d \mathbf{m}_d^R e^{i\mathbf{Q}\cdot\mathbf{r}_d}, \quad \mathbf{P}(\mathbf{Q}) = \hat{\mathbf{Q}} \times (\hat{\mathbf{e}} \times \hat{\mathbf{Q}}). \qquad (2)$$

Here $\mathbf{m}_d^R$ is the magnetic moment of the ion at site $d = 1,\ldots,4$ in the symmetry class R, $\hat{\mathbf{Q}}$ is the unit vector along the neutron momentum transfer, and $\hat{\mathbf{e}}$ is the unit vector along $\mathbf{m}_d^R$. For each of the three peaks, Table I lists $|F_R(\mathbf{Q})|^2$ (normalized to unit magnetic moment) and $|P(\mathbf{Q})|^2$ for $R = C, A, G, F$ and all spin directions $\hat{\mathbf{e}}$ parallel to x, y, or z. The numbers represent the sensitivity of each peak to the different basis structure components. As presented in Fig. 3(a), the extension of the neutron-diffraction experiments has now shown that there is intensity in the $(1,k_{\mathrm{ic}},0)$ reflection. This reflection derives mainly from an A_y or an A_z component according to Table I. The intensity disappears below and not at $T_{\mathrm{N}} \approx 20.8$ K indicating the presence of a second magnetic phase transition at about 17.7 K. Referring to Eq. (1) it is seen that the order parameter between 17.7 K and T_{N} belongs to the irreducible Γ_1 representation, whereas the new order parameter appearing below 17.7 K has the symmetry of the Γ_2 or the Γ_3 representation depending on whether the $(1,k_{\mathrm{ic}},0)$ peak is due to, respectively, an A_y or an A_z component. The temperature dependence of the strong peak intensity at $(0,1+k_{\mathrm{ic}},0)$ is depicted in Fig. 3(c), and Table I shows that the two components C_z and C_x are weighted equally and are the only ones appearing in this scan. The abrupt increase shown by the $(0,1+k_{\mathrm{ic}},0)$ peak intensity at 17.7 K for decreasing temperatures allows a clear choice between the two possibilities for the new order parameter. A Γ_3 order parameter, which contains a C_x component, contributes directly to the $(0,1+k_{\mathrm{ic}},0)$ peak, whereas the possibility of a Γ_2 order parameter can be dismissed since it has no direct effect on this scan. The behavior of the $(1,2+k_{\mathrm{ic}},0)$ intensity as a function of temperature shown in Figs. 3(b) and 3(c) is consistent with this result. This peak intensity reflects the A_x and A_z components, and for increasing temperatures it shows a rapid drop at 17.7 K indicating a vanishing A_z component. The intensity, which remains above 17.7 K, is due to the A_x component being nonzero up to T_{N}. Table I shows that both the $(1,k_{\mathrm{ic}},0)$ and the $(1,2+k_{\mathrm{ic}},0)$ peak may contain contributions from the possible G components. However, since none of the peaks which are dominated by the G components have been seen, they may safely be neglected here, where their contributions are weighted with an intensity factor of 1/40 compared with the A components.

TABLE I. Squared structure (F) and polarization (P) factors for the three IC peaks used to establish the spiral structure in terms of the irreducible representations. The structure factors are normalized to unit spin lengths of the components. We have used $k_{\mathrm{ic}} = 0.18$ r.l.u., but note that small changes of k_{ic} have no effect on our conclusions.

	F_C^2	F_A^2	F_G^2	F_F^2	P_x^2	P_y^2	P_z^2
$(0,1+k_{\mathrm{ic}},0)$	16	0	0	0	1	0	1
$(1,k_{\mathrm{ic}},0)$	0	15.6	0.4	0	0.09	0.91	1
$(1,2+k_{\mathrm{ic}},0)$	0	15.6	0.4	0	0.93	0.07	1

Generally, a helical/cycloidal ordering is energetically more favorable than a linearly polarized square wave of fully polarized spins in the $T = 0$ limit, as long as the anisotropy within the plane of the ordered moments is weak. In the present case the system may approach a circular polarization of the moments by either combining the C_z component with a C_x or with a C_y component. The unique identification above, that the new order parameter below 17.7 K belongs to the Γ_3 representation, shows that the system chooses the

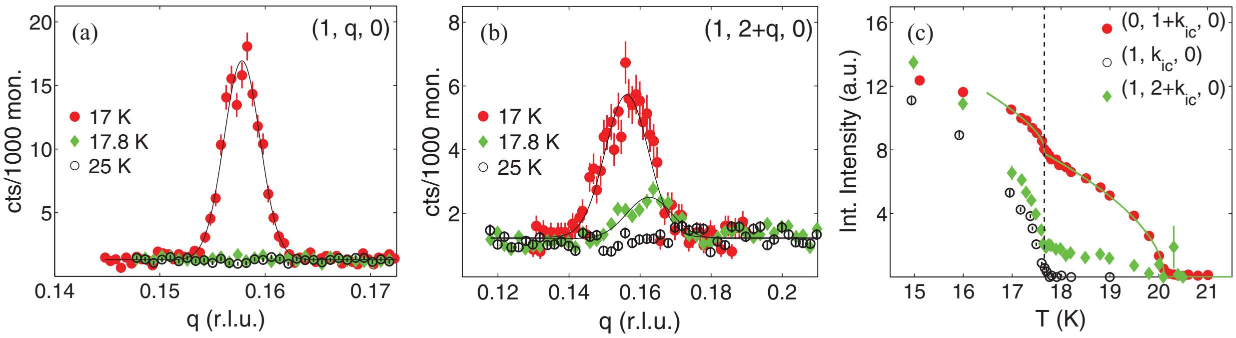

FIG. 3. (Color online) (a), (b) Neutron-diffraction scans through the $(1,k_{\rm ic},0)$ and the $(1,2+k_{\rm ic},0)$ peaks at 14.7 T applied along the c axis at temperatures close to the transition at 17.7 K. The two peaks reflect, respectively, the A_z (neglecting A_y as discussed in the text) and the weighted sum of the A_z and A_x components of the spiral structure. The A_z component disappears above 17.7 K while the A_x component persists. (c) Integrated intensities of $(0,1+k_{\rm ic},0)$, $(1,k_{\rm ic},0)$, and $(1,2+k_{\rm ic},0)$ as functions of temperature at 14.7 T applied along the c axis. The integrated intensity from the $(1,k_{\rm ic},0)$ and the $(1,2+k_{\rm ic},0)$ peaks have been multiplied by a factor of 140 and 170, respectively. The onset of an additional order parameter below 17.7 K is evident.

first one of the two possibilities. This choice is consistent with the fact that the anisotropy parameters derived from the spin-wave analysis [see Eq. (5) below] identifies the ac plane to be the easy one. Experimentally, it is difficult to measure the C_y component directly but the analysis above, where the irreducible representations, or symmetry arguments, are utilized in the interpretation of the experiments, indicates that Γ_4, and thereby the C_y component, has to be zero. This result is also valid at the lower temperatures not included in Fig. 3, since the $(1,k_{\rm ic},0)$ peak indicating a nonzero Γ_3 component is observed all the way down to 2 K.

We conclude that the system shows two continuous phase transitions at decreasing temperatures in the presence of a c-axis field larger than 13.5 T. The ordered state just below $T_{\rm N}$ is described by an IC order parameter belonging to the irreducible representation Γ_1, with the dominating component C_z being slightly mixed with A_x. At about 17.7 K there is a new second-order phase transition, where the additional order parameter belongs to the Γ_3 representation and may be described as being the C_x component slightly mixed with the A_z component. The diffraction experiments do not allow a determination of the phases of the two order parameters, but the only relevant possibility is that the phases of the two components differ by 90°, since an elliptical polarization minimizes the variation of the lengths of the ordered moments. This interpretation of the observations shown in Fig. 3 is in full agreement with the predictions of the MF calculations presented below. The phase boundary between the linearly and elliptically polarized IC phases has been determined up to a field of 17.3 T. The two IC structures are illustrated in Figs. 6(a) and 6(c), and the observed phase boundaries are shown in the phase diagram in Fig. 4.

C. The high-field IC–C transition

At the V2/FLEX triple-axis spectrometer we measured the IC modulation $k_{\rm ic}$ for fields along c in the range $13\ {\rm T} < \mu_0 H < 17.3\ {\rm T}$ and for temperatures up to $T_{\rm N}$. To obtain an accurate value of $k_{\rm ic}$, both symmetry-related peaks $(0,1\pm k_{\rm ic},0)$ were measured, optimizing the sample rotation and the scattering angle thoroughly and obtaining $k_{\rm ic}$ as the average modulation of the two peaks. The modulation as a function of magnetic field at 2 K and as a function of temperature at 17.3 T is shown in Fig. 5. It is seen that the modulation stabilizes at $k_{\rm ic} = \frac{1}{5}$ at 2 K for $\mu_0 H > 16$ T marking a magnetic quintupling of the unit cell. At 17.3 T, the quintupling persists up to 10 K. The average measured value of the modulation in this phase is $k_{\rm ic} = 0.200(1)$. The accuracy of the determined value of

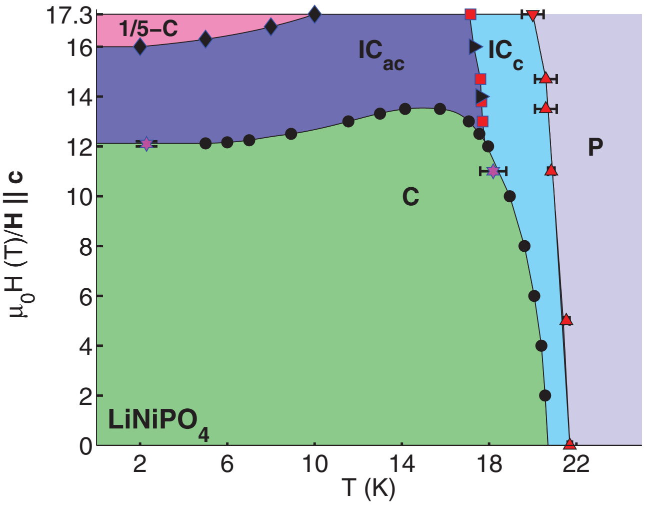

FIG. 4. (Color online) $(\mu_0 H,T)$-phase diagram of LiNiPO$_4$ for magnetic fields applied along the c axis. The black circles mark the C–IC phase boundary as found using magnetization data, supported by neutron-diffraction data taken from Ref. 7 (stars). The diamonds mark the lock-in phase boundaries found using V2/FLEX data. The squares mark the boundary of the IC spiral phase found at RITA-II (below 15 T) and V2/FLEX (above 15 T), while the two right-pointing triangles indicate the phase boundary detected by VSM measurements. The ordering temperatures of the linearly polarized IC phase are taken from Ref. 7 (up-pointing triangles) and are supported by a measurement from V2/FLEX (down-pointing triangle). The errors on the VSM measurements are much smaller than the markers, while the error bars on the neutron-diffraction measurements are comparable to the marker size if not explicitly given. IC$_{\rm c}$ denotes the IC structure linearly polarized mainly along c, while IC$_{\rm ac}$ denotes the IC spiral in the ac plane. C denotes the commensurate AFM phase and 1/5-C denotes the commensurate lock-in spiral phase.

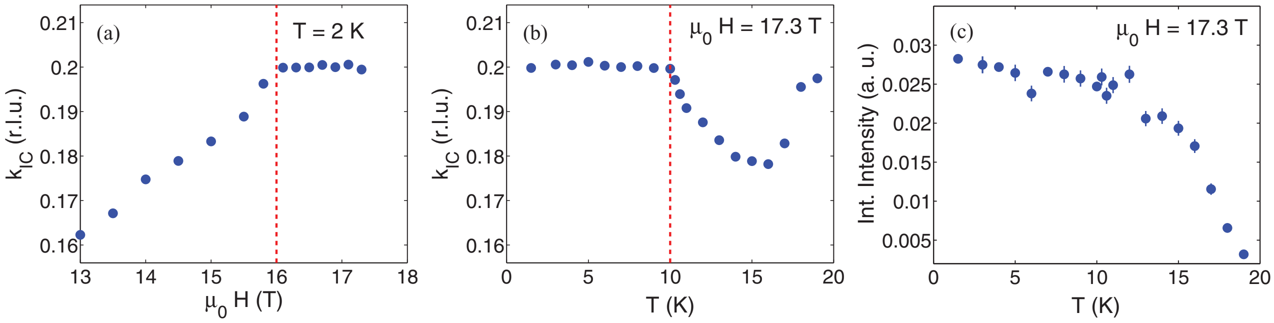

FIG. 5. (Color online) The IC modulation k_{ic} as a function of field at 2 K (a) and as a function of temperature at 17.3 T applied along the c axis (b). The statistical errors are smaller than the markers. (c) The temperature dependence of the sum of integrated intensities from the symmetry-related peaks $(0,1 \pm k_{\mathrm{ic}},0)$ measured at 17.3 T applied along the c axis.

k_{ic} is comparable to the obtainable instrumental precision. In addition, k_{ic} was measured as a function of field at 5 K and as a function of temperature at 16.8 T.

The $(1,k_{\mathrm{ic}},0)$ peak reflecting the A_z component is still observed above 16 T at 2 K (not shown), which indicates that the magnetic structure stays as an elliptical spiral at the transition from the IC phase to the high-field commensurate phase. The lock-in transition identified here explains the $\mu_0 H \simeq 16$ T transition observed by Khrustalyov *et al.*,[17] and the weakness of the signal they observed at this transition is consistent with that the lock-in only causes minor modifications of the magnetic structure. The commensurate magnetic spiral structure is shown in Fig. 6(b). The phase boundary between the IC spiral phase and the high-field commensurate spiral phase is included in the phase diagram shown in Fig. 4.

D. Phase boundaries determined from bulk magnetization measurements

Figure 7 shows the magnetization at 5 K as a function of applied field along all three crystallographic axes. The magnetization is almost linear along the a and b axes. Along the c axis the magnetic susceptibility is much smaller until the system enters the IC canted spiral phase at 12.2 T, where there is a fivefold increase of the magnetization. The transition is first order and hysteretic. We define the C–IC phase boundary in field scans as the field at which the differential magnetization dM/dH, measured for increasing fields, exhibits a maximum.

The IC–C phase boundary for fields applied along the c axis was determined by performing a series of VSM measurements at constant field while varying temperature and vice versa. Figure 8 shows the magnetization as a function of temperature at $\mu_0 H = 12.5$ T. Below T_{N} when the system is in the canted linearly polarized IC phase, the magnetization is gradually decreasing with decreasing temperatures. This is followed by a sudden drop in magnetization when entering the C phase at 17 K. At 9 K the magnetization increases rapidly upon entry into the canted spiral phase. The first-order nature of the transitions in and out of the C phase is evident from the significant hysteresis. We define the phase boundaries in temperature scans to be the points of maximal or minimal differential magnetization upon cooling.

The transition from the structure with linearly polarized moments to the canted IC spiral can be seen directly in the VSM measurements. Figure 9 shows the temperature dependence of the magnetization at $\mu_0 H = 16$ T, measured upon cooling, in which two distinct kinks are evident: one at the ordering temperature T_{N}, where IC magnetic order sets in, and one at $T = 17.3$ K, where the spins start to develop a C_x component. The differential magnetization shows two distinct peaks, indicating the two second-order phase transitions from

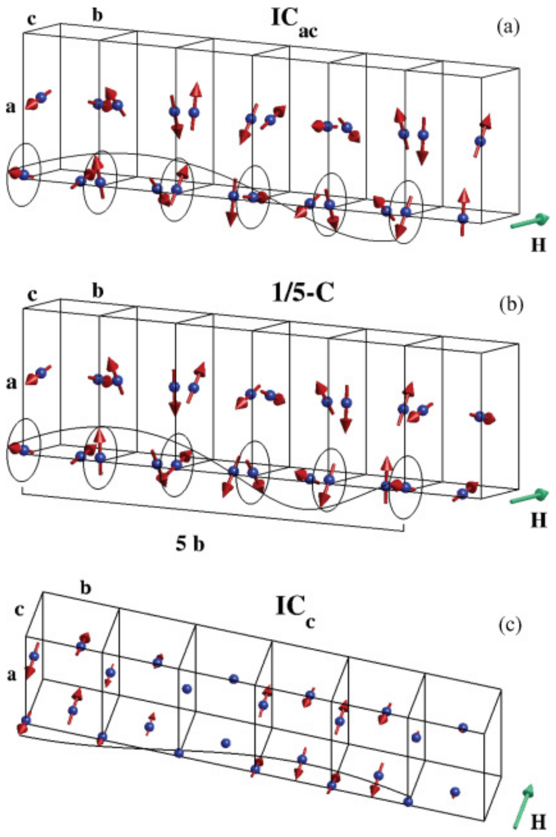

FIG. 6. (Color online) The three magnetic IC structures shown by stacking six unit cells along b. Only the four magnetic Ni^{2+} ions are shown in each unit cell. (a) Magnetic IC spiral at 2 K and $\mu_0 H = 13$ T applied along c. The circles around the lower left ion marks the rotation plane of the spins and the black line marks the spiral itself. (b) Lock-in commensurable spiral $\mu_0 H > 16$ T and $T < 10$ K. The 1/5 modulation is evident by comparing the 1st and the 6th unit cell. (c) Linearly polarized IC structure; the line marks the sinusoidal modulation. In the phase diagram for fields along c, shown in Fig. 4, the three structures are denoted as $\mathrm{IC}_{\mathrm{ac}}$, 1/5-C, and IC_{c}, respectively.

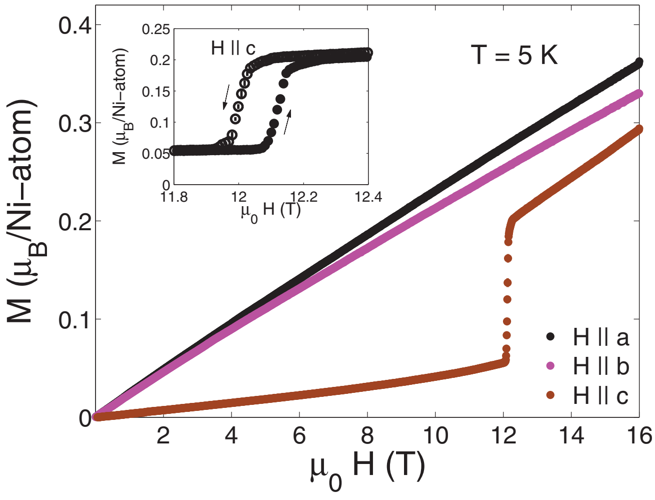

FIG. 7. (Color online) Magnetic field dependence of the magnetization measured along all three crystallographic axes at 5 K and for increasing fields. The inset zooms in on the hysteric C–IC transition observed for fields along c.

the paramagnetic phase to the linear IC structure (T_N) and from the linear to the spiral IC structure. Combining our neutron-diffraction and magnetization measurements with neutron-diffraction results from Ref. 7, we present a complete phase diagram of LiNiPO$_4$ for c-axis fields $\mu_0 H < 17.3$ T in Fig. 4.

The phase diagrams for fields along the a and b axes have also been determined. The field leads to minor decreases in T_N and T_{NC}, but no other phase transitions than the paramagnetic–IC and the IC–C transitions were detected. Figure 10 shows the phase diagram obtained from magnetization measurements, when the field is applied along the b axis. The inset shows that there is a small kink in the differential magnetization at T_N followed by a large peak at T_{NC}, where the system becomes commensurate. The phase diagram for fields applied along the a axis is identical within errors to that for fields along b.

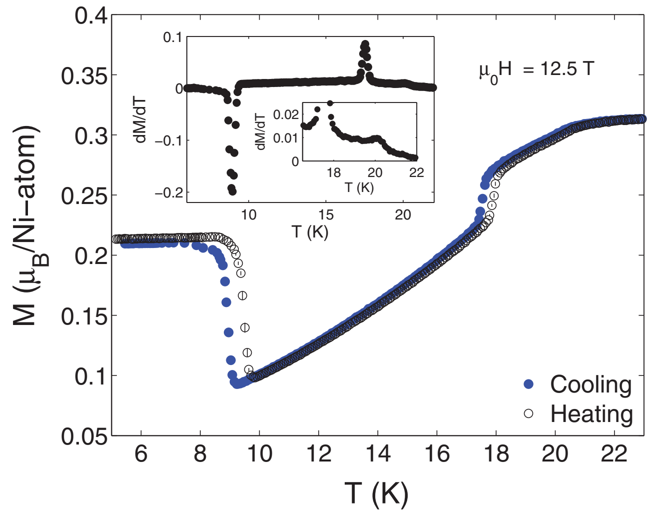

FIG. 8. (Color online) The temperature dependence of the magnetization at 12.5 T applied along the c axis. The insets show the differential magnetization upon cooling with an additional focus on the kink at T_N.

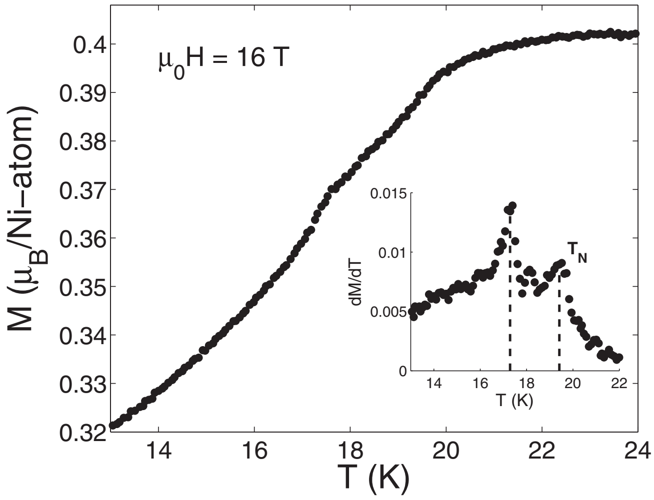

FIG. 9. Magnetization measured while cooling at a field of $\mu_0 H = 16$ T applied along the c axis. Two kinks are evident. The inset shows the derivative, where two transitions are marked by dashed lines.

IV. MODEL CALCULATIONS

A. The mean-field model and the RPA

The Ni ions in LiNiPO$_4$ constitute an $S = 1$ system, where the orbital perturbation gives rise to a slight increase of the effective g factor and an effective anisotropy field acting on the spins. According to experiments the saturated ordered moment is about 2.2μ_B/Ni-ion in the limit of zero temperature,[7] and the Hamiltonian is assumed to be

$$\mathcal{H} = \frac{1}{2}\sum_{ij} J(ij)\mathbf{S}_i \cdot \mathbf{S}_j + \mathcal{H}_{\mathrm{DM}} + \sum_{\alpha,i} D_\alpha S_{\alpha i}^2 - g\mu_B \sum_i \mathbf{H}\cdot\mathbf{S}_i \qquad (3)$$

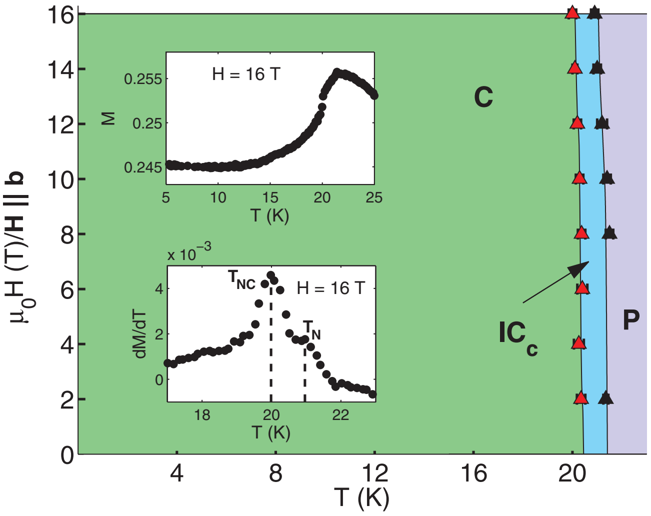

FIG. 10. (Color online) ($\mu_0 H,T$)-phase diagram determined from bulk magnetization measurements for fields applied along the b axis. The insets shows the magnetization and the differential magnetization at 16 T, where the transitions at T_N and T_{NC} are marked. IC$_c$ denotes the IC structure linearly polarized mainly along c.

with $g = 2.2$. The possible occurrence of anisotropic exchange terms is considered to be dominantly due to the Dzyaloshinsky-Moriya (DM) mechanism. Assuming that only nearest neighbors contribute, the DM interaction allowed by symmetry is[11,15]

$$\mathcal{H}_{\mathrm{DM}} = D_{14} \sum_{ij\in \mathrm{n.n.}} [S_z(1i)S_x(4j) - S_x(1i)S_z(4j) + S_z(3i)S_x(2j) - S_x(3i)S_z(2j)], \qquad (4)$$

where, e.g., $S_z(1i)$ only contributes to the sum if the ith site belongs to sublattice 1. The exchange constants and the single-ion anisotropy constants, D_x and D_y, were all deduced from the low-temperature spin waves in Ref. 11. We have repeated the spin-wave analysis using the more general RPA method presented in Ref. 19. The actual procedure used here is the same as used in the RPA analyses of the magnetic excitations in the two systems $\mathrm{HoF_3}$ and PrNiSn,[20,21] which belong to the same space group as $\mathrm{LiNiPO_4}$. The MF/RPA theory is obtained to zero order in the high-density $1/z$ expansion, and the corrections appearing in the first order of $1/z$ are discussed in Ref. 22 for the case of $\mathrm{HoF_3}$. The energies and scattering intensities of the spin waves in $\mathrm{LiNiPO_4}$, and the exchange constants derived here, agree with the results determined previously when applying the linear spin-wave theory,[11] except that the values of the anisotropy constants are slightly modified into (in units of meV)

$$D_x = 0.413, \quad D_y = 1.423, \quad D_{14} = \pm 0.32 \qquad (5)$$

($D_z = 0$). This shows that the c axis is the preferred direction for the spins, and that the b axis is the hardest. The DM anisotropy has no effect on the spin waves to leading order,[11,15] and D_{14} is not determined from the spin waves but from the experimental value of $|\theta| = 7.8^\circ \pm 2.6^\circ$,[7] where θ is the canting angle the ordered moments are making with the c axis in the zero field and temperature limit. The canting may just as well be reproduced, if the DM term is replaced by the single-ion anisotropy term $\pm B_2^1(S_zS_x + S_xS_z)/2$ with $B_2^1 \approx 2.5$ meV. However, we find that this large single-ion anisotropy has unfavorable effects on the spin-wave energies, and that the amplitudes of the higher harmonics of the moments in the IC phase become much larger than observed. Although the DM anisotropy derived here is surprisingly large (about one-third of the corresponding exchange interaction), it is likely that this is the dominating interaction determining the canting. The canting angle has a definite sign, depending on the sublattice considered, but this is difficult to detect experimentally, and the sign of D_{14} is left unspecified.

The susceptibility components have been calculated within the MF approximation and are compared with our experimental results in Fig. 11. In order to get these results we have introduced one more exchange constant in the model in addition to the five constants given in Table I in Ref. 11. The exchange coupling J_b^c between an ion at $\mathbf{r}_i$ and its four diagonal neighbors belonging to the same sublattice, at $\mathbf{r}_i \pm \mathbf{b} \pm \mathbf{c}$, is assumed to be ferromagnetic with the value -0.23 meV. This has been done without changing $J(\mathbf{q})$ along the directions of $\mathbf{q}$ where the spin waves have been measured, by replacing J_b and J_c with, respectively, $J_b' = J_b - 2J_b^c = 1.13$ meV and $J_c' = J_c - 2J_b^c = 0.4$ meV. The six exchange parameters used in the present calculations are given in Table II. The transition temperature predicted by the MF model is about 32 K, i.e., 10 K above the experimental one. The exchange parameters determined from the spin waves in the zero-temperature limit are close to be the true ones, and in terms of these exchange parameters the MF estimate of T_N is expected to be of the order of 10%–30% higher than the true ordering temperature. Hence, it is plausible that most of the discrepancies in Fig. 11 are due to the MF approximation. Outside the critical regime the MF model accounts reasonably well for the experimental results, which means that the values for $J_F(\mathbf{0})$ and the anisotropy constants D_x and D_y derived from the spin waves are trustworthy.

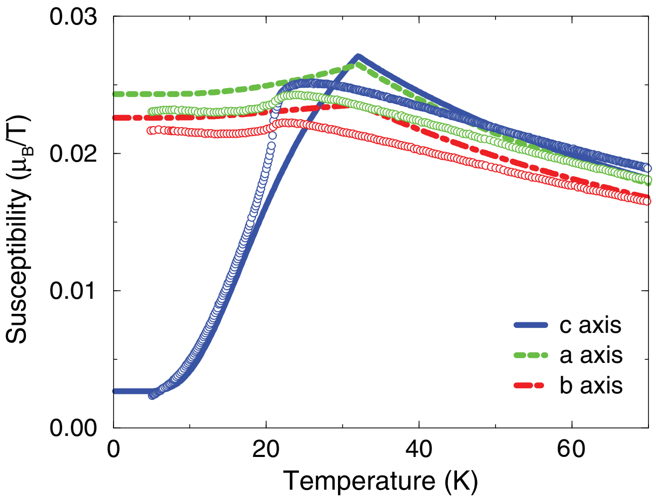

FIG. 11. (Color online) The calculated susceptibility components (solid lines), divided by μ_0, are compared with the experimental results obtained from our magnetization measurements after being corrected for a trace of paramagnetic impurities. The experimental results are consistent with those obtained by Kharchenko *et al.*[23] and the powder susceptibility measurements by Vaknin *et al.*[24]

The RPA theory reproduces all the linear spin-wave theory results derived in Ref. 11 in the zero field and temperature limit. The present numerical method is straightforwardly generalized to account for the different complications—the canting of the spins due to D_{14} and the introduction of nonzero values of temperature and fields. In Fig. 12 is shown a comparison between theory and experiments when applying a field at 2 K, whereas Fig. 13 focuses on the temperature effects at zero field. Except that the MF/RPA theory may not be trusted close to T_N, the comparisons shown in the two figures are quite satisfactory.

TABLE II. The exchange parameters (in units of meV) derived from the experimental dispersion relations. The first row shows the number of neighbors (Z) and the second one the distances d between the ions.

	J_{bc}	J_b'	J_c'	J_{ab}	J_{ac}	J_b^c
Z	4	2	2	$2+2$	$2+2$	4
d (Å)	3.77	4.66	5.83	5.46/5.60	5.36/6.25	7.46
$J(ij)$	1.002	1.13	0.40	0.321	-0.112	-0.23

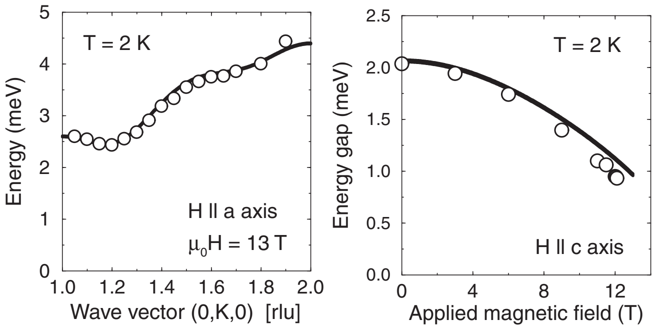

FIG. 12. Spin waves at 2 K. The left figure shows the calculated dispersion relation along $(0,K,0)$ at a field of 13 T applied along the a direction compared with the experimental results. The spin-wave energy gap at $(0,1,0)$ as a function of a field applied along the c axis is compared with experiments performed by Strauss *et al.* (Ref. 25) in the right figure.

The exchange parameters at zero wave vector are derived to be (in meV) $J_F(\mathbf{0}) = 6.98$, $J_C(\mathbf{0}) = -3.60$, $J_A(\mathbf{0}) = 5.31$, and $J_G(\mathbf{0}) = -0.14$ for the four different symmetry configurations. These numbers show that the C configuration is the most favorable one, whereas the exchange interaction strongly opposes the A and F configurations. This is the situation at zero wave vector, but this is not changed much in the IC phase ($k_{\rm ic}$ is small). The c axis is the easy axis, and accordingly the ordered phase just below $T_{\rm N}$ is dominantly determined by the C_z configuration. That it is A_x rather than G_y which is accompanying the C_z component is not explained alone by the circumstance that the y (b) axis is the hard axis, but is due to the relatively large DM anisotropy favoring A_x. It is worth pointing out that any first-order DM interaction between a y component of a spin and a z or x component of a neighboring spin cancels by symmetry.[15] This means that the G_y component may only be coupled with the (C_z,A_x) components due to orbital modifications of the exchange integrals that are of second order in the spin-orbit coupling. Furthermore, the possible couplings between G_y and the two other IC components are forced to vanish by symmetry in the limit of $k_{\rm ic} \to 0$.

The energy minimum in the spin-wave dispersion along $(0,K,0)$ is very shallow (see Figs. 12 and 13) showing that the difference between $J_C(\mathbf{k}_{\rm ic})$ and $J_C(\mathbf{0})$ is minute. The extra lock-in energy gained by the system at zero wave vector, where the lengths of the moments are no longer varying, is able to compensate for this energy difference already 1 K below $T_{\rm N}$, by which temperature $T_{\rm NC}$ the IC phase is being replaced by the corresponding uniform C phase. In the zero-temperature limit, the MF model predicts the first-order IC–C transition to occur at about the same c axis field, $\mu_0 H \approx 13$ T, as observed, and also that the structure in the IC phase is elliptically polarized by combining components from two one-dimensional irreducible representations, (C_z,A_x) and, 90° out of phase and with a slightly smaller amplitude, (C_x,A_z). In this way the IC structure is able to maintain a nearly constant length of the ordered moments by a slight cost in anisotropy energy (notice that the anisotropy within the ac plane is rather weak), which makes it competitive with the C structure. When the temperature is increased, at a constant c-axis field, the anisotropy within the ac plane implies that the (C_x,A_z) moment decreases faster than the main component, and the MF model predicts that it vanishes 2–3 K below $T_{\rm N}$ in agreement with the experimental phase diagram. There have been some preliminary investigations of the higher harmonics in the IC phase,[25] and the intensity due to the third harmonic of the C_z component is observed to be about 10^{-3} times the peak intensity due to the first harmonic in the zero-temperature limit. Once again this is in qualitative agreement with the results derived from the MF model. At least, the possibility that the linearly polarized structure should be the stable one at zero temperature can be excluded, since the observed intensity ratio is much smaller than the value of $\sim 1/9$ expected for a linearly polarized squared-up structure.

The energies involved in the gradual changes of $k_{\rm ic}$ and in the lock-in transition to the commensurate 1/5 phase are too small to be modeled by the present MF calculations. However, the model does predict the presence of two additional transitions, one at a c-axis field of about 18 T and another one at about 20 T in the zero-temperature limit. We anticipate that these two transitions are just those observed by Khrustalyov *et al.*[17] at 20 and 21 T (numbered 4 and 5 in their Fig. 1). If this is true, the model calculations show that the one at 20 T is due to a continuous but very rapid change of the higher harmonics (the most pronounced changes are shown by the zeroth and second harmonics of the C_z and C_x components), whereas the second transition is due to smaller but abrupt modifications of all the higher harmonics.

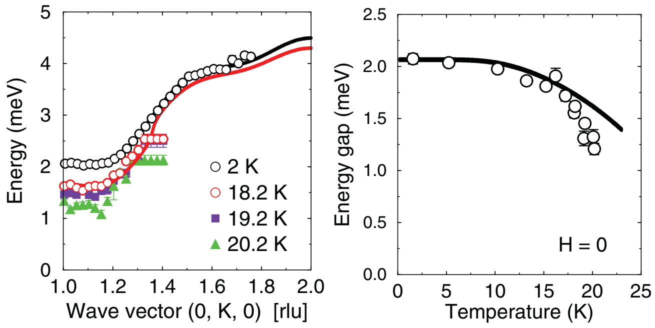

FIG. 13. (Color online) Spin waves at zero field. The figure to the left shows the RPA dispersion relation along $(0,K,0)$ as a function of temperature in comparison with experimental results. To the right is shown a comparison between observations and calculations of the spin-wave energy gap at $(0,1,0)$ as a function of temperature.

B. Spin dynamics in the high-field IC spiral phase

The spin waves have been studied experimentally in the high-field IC spiral phase. The incommensurable ordering implies that the excitation spectrum should contain a Goldstone mode reflecting that an overall phase shift of the spiral does not cost any energy. To investigate this phenomenon we have performed a number of inelastic neutron scattering experiments around the magnetic Bragg peak at low energies (above ~ 0.4 meV). These results are compared with the RPA predictions derived from the MF model in Figs. 14 and 15.

The numerical RPA method discussed above is straightforwardly generalized to the case where the magnetic unit

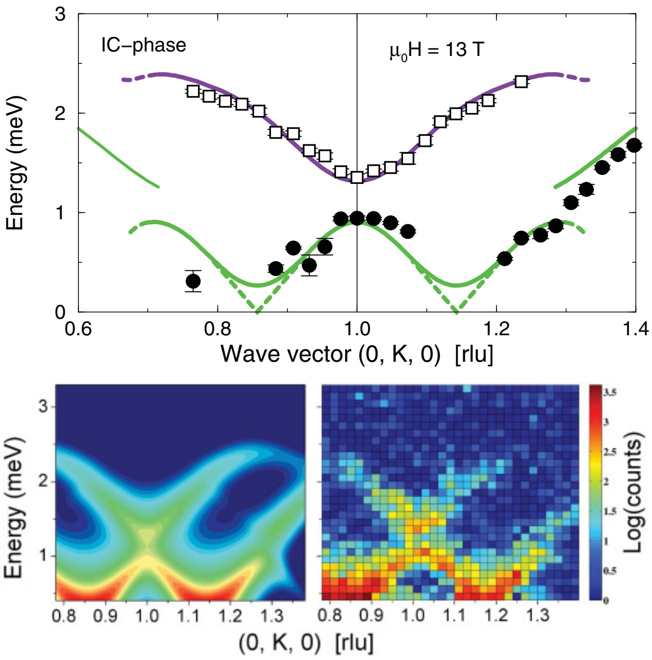

FIG. 14. (Color online) The low-energy spin-wave dispersions measured along $(0,K,0)$ in the IC phase at 2 K and in a 13 T field applied along the c axis. The circles and squares in the upper figure show the experimental results. The solid lines are the predictions of the RPA in the case of $k_{\mathrm{ic}} = 1/7$, whereas the dashed straight lines indicate the Goldstone modes expected for an incommensurate structure. The two figures below are the corresponding logarithmic contour plots of the scattering intensities along $(0,K,0)$. The experimental results are shown to the right to be compared with the calculated results shown in the left figure.

cells contains any integer multiple of 4 spins.[19] The numerical method presupposes a commensurable ordered structure, but the results may still be valid for describing an incommensurate system, if the commensurable period assumed in the calculations is sufficiently long. The most significant effect of the assumption of commensurability is that the excitations are going to exhibit a nonzero energy gap at the ordering wave vector instead of the soft-mode behavior expected in the incommensurable case. In the calculations shown in Figs. 14 and 15, we have assumed an ordered magnetic structure with a period of 7 crystallographic unit cells along the b axis, which in the model leads to an energy gap of about 0.25 meV at the ordering wave vector. Outside the close neighborhood of the magnetic Bragg points at $(0,1 \pm k_{\mathrm{ic}},0)$, the assumption of commensurability is unimportant and the RPA predictions are found to be in nearly complete agreement with the experimental results, both with respect to the energies and the scattering intensities of the magnetic excitations. The most important energy gap induced by the IC ordering is the one at $(0,1,0)$, but also the presence of the smaller, higher-order one calculated at about $(0,1 \pm 0.3,0)$ has been verified by a direct observation of a two-peak scattering structure in a constant q scan at $(0,1.3,0)$.

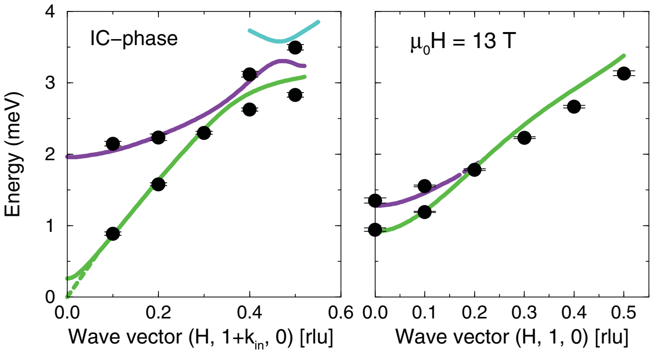

FIG. 15. (Color online) Spin-wave dispersions in the IC phase at 2 K and 13 T along $(H,1+k_{\mathrm{ic}},0)$ and $(H,1,0)$. The symbols are the same as used in Fig. 14.

We have made attempts to look for inelastic scattering peaks also outside the (q,ω) regime covered by Figs. 14 and 15 with no success. This is, once more, consistent with the RPA calculations, since they indicate that the magnetic peaks become very weak, in practice invisible, at the higher energies.

V. CONCLUSIONS

We have used neutron diffraction to identify two new magnetic phases in LiNiPO$_4$, induced by the application of magnetic fields larger than 12 T along the c axis. In the process, we have clarified the magnetic phase diagram for fields up to 17.3 T along c, and, from magnetization measurements, the phase diagrams for fields up to 16 T along a and b. For fields along c, the IC modulation vector $(0,k_{\mathrm{ic}},0)$ was shown to stabilize at a commensurate value $(0,\frac{1}{5},0)$ for fields larger than 16 T below 10 K. We presented an irreducible-representation analysis of our neutron-diffraction data, which is consistent with a temperature-driven continuous phase transition from a low-temperature, elliptically polarized, canted IC spiral to a high-temperature, linearly polarized, canted IC structure. This phase transition was also resolved in our bulk magnetization data, and the transition temperatures derived from magnetization and neutron-diffraction data were found to agree within experimental error.

The mechanism proposed in Ref. 7 for the ME effect in LiNiPO$_4$ gives rise to an electric polarization in the C phase, when applying a field along the a or the c axis, but not in the IC phases. These predictions are consistent with observations in the C and low-field IC phases.[8,9,14] The combination of the Γ_1 and Γ_3 order parameters in the high-field IC phase may lead to additional ME effects, but since the main (C,A) components of the spiral are all perpendicular to the ordering wave vector,[26] the ME effects related to the spiraling ordering are expected to cancel out.

The MF model presented here is determined from the analysis in Ref. 11 of the spin waves observed at 2 K and zero field. The excellent account of the spin waves obtained under these conditions has here been extended so to comprise the spin waves observed at nonzero values of temperatures and fields in the uniformly ordered C phase. In the IC phase at low temperatures and high fields, we have observed well-defined magnetic excitations at energies below 3–4 meV, which carry substantial intensity only for wave vectors in the vicinity of the incommensurate ordering vectors. All of these observations are in firm agreement with the RPA predictions. In spite of the limited validity of the MF approach close to a second-order phase transition, the present MF model predicts a phase diagram in good agreement with our observations. Most importantly, the MF predictions have been a valuable guidance in the determination of the magnetic structures in the different phases. In spite of its success, the MF model also shows some failures. The calculated and observed intensity ratios between different components and harmonics are found to differ in a number of cases. Some of these discrepancies might be due to the MF approximation itself, but there are systematic features indicating that the model needs to be improved, i.e., that the anisotropic modifications of the exchange interactions, appearing in the second order of the spin-orbit coupling, may be of some importance. This conclusion is substantiated by the large value of the leading-order DM interaction derived in the present analysis.

ACKNOWLEDGMENTS

Work was supported by the Danish Agency for Science, Technology, and Innovation under DANSCATT and by the Swiss NSF via Contract No. PP002-102831. The manuscript has been authored, in whole or in part, under Contract No. DE-AC02-07CH11358 with the US Department of Energy. Neutron experiments were performed at the SINQ neutron spallation source at the Paul Scherrer Institute, Switzerland, and at the Berlin Neutron Scattering Center (BENSC) at the Helmholtz Zentrum Berlin, Germany.

---

[1] S. W. Cheong and M. Mostovoy, Nature Mater. **6**, 13 (2007).

[2] M. Fiebig, J. Phys. D: Appl. Phys. **38**, R123 (2005).

[3] W. Eerenstein, N. D. Mathur, and J. F. Scott, Nature (London) **442**, 759 (2006).

[4] T. Kimura, T. Goto, H. Shintani, K. Ishizaka, T. Arima, and Y. Tokura, Nature (London) **426**, 55 (2003).

[5] G. Lawes, A. B. Harris, T. Kimura, N. Rogado, R. J. Cava, A. Aharony, O. Entin-Wohlman, T. Yildrim, M. Kenzelmann, C. Broholm, and A. P. Ramirez, Phys. Rev. Lett. **95**, 087205 (2005).

[6] M. Kenzelmann, A. B. Harris, S. Jonas, C. Broholm, J. Schefer, S. B. Kim, C. L. Zhang, S.-W. Cheong, O. P. Vajk, and J. W. Lynn, Phys. Rev. Lett. **95**, 087206 (2005).

[7] T. B. S. Jensen, N. B. Christensen, M. Kenzelmann, H. M. Rønnow, C. Niedermayer, N. H. Andersen, K. Lefmann, J. Schefer, M. v. Zimmermann, J. Li, J. L. Zarestky, and D. Vaknin, Phys. Rev. B **79**, 092412 (2009).

[8] M. Mercier, Ph.D. thesis, Université de Grenoble, 1969.

[9] I. Kornev, M. Bichurin, J.-P. Rivera, S. Gentil, H. Schmid, A. G. M. Jansen, and P. Wyder, Phys. Rev. B **62**, 12247 (2000).

[10] I. E. Chupis, Low Temp. Phys. **26**, 419 (2000).

[11] T. B. S. Jensen, N. B. Christensen, M. Kenzelmann, H. M. Rønnow, C. Niedermayer, N. H. Andersen, K. Lefmann, M. Jiménez-Ruiz, F. Demmel, J. Li, J. L. Zarestky, and D. Vaknin, Phys. Rev. B **79**, 092413 (2009).

[12] I. Abrahams and K. S. Easson, Acta Crystallogr. Sect. C **49**, 925 (1993).

[13] R. P. Santoro, D. J. Segal, and R. E. Newnham, J. Phys. Chem. Solids **27**, 1192 (1966).

[14] D. Vaknin, J. L. Zarestky, J.-P. Rivera, and H. Schmid, Phys. Rev. Lett. **92**, 207201 (2004).

[15] T. B. S. Jensen, Ph.D. thesis, Risø National Laboratory, 2007.

[16] The two transition temperatures T_{N} and T_{NC} were named, respectively, T_{IC} and T_{N} in some of the previous publications on $\mathrm{LiNiPO_4}$. Here we prefer to refer to the temperature at which long-range order first appears as T_{N}.

[17] V. M. Khrustalyov, V. N. Savitsky, and N. F. Kharchenko, Czech. J. Phys. Suppl. D **54**, 27 (2004).

[18] J. Rossat-Mignod, in *Methods of Experimental Physics*, Part C, Chap. 19, Vol. 23 (Academic Press, Inc., 1987).

[19] J. Jensen and A. R. Mackintosh, *Rare Earth Magnetism: Structures and Excitations* (Clarendon Press, Oxford, 1991).

[20] M. J. M. Leask, M. R. Wells, R. C. C. Ward, S. M. Hayden, and J. Jensen, J. Phys. Condens. Matter **6**, 505 (1994).

[21] K. A. McEwen, J. Jensen, E. D. Beirne, J. P. Allen, K. Habicht, D. T. Adroja, R. I. Bewley, and D. Fort, Phys. Rev. B **73**, 014402 (2006).

[22] J. Jensen, Phys. Rev. B **49**, 11833 (1994).

[23] Yu. N. Kharchenko, N. F. Kharcheno, M. Baran, and R. Szymczak, Low Temp. Phys. **29**, 579 (2003).

[24] D. Vaknin, J. L. Zarestky, J. E. Ostenson, B. C. Chakoumakos, A. Goni, P. J. Pagliuso, T. Rojo, and G. E. Barberis, Phys. Rev. B **60**, 1100 (1999).

[25] A. B. Strauss, M. H. Madsen, E. Brok, J. V. Pedersen, and P. Krogstrup (unpublished NBI report).

[26] M. Mostovoy, Phys. Rev. Lett. **96**, 067601 (2006).